Seasonal Influence of Indonesian Throughflow in the Southwestern Indian Ocean

LEI ZHOU AND RAGHU MURTUGUDDE

Earth System Science Interdisciplinary Center, College Park, Maryland

MARKUS JOCHUM

National Center for Atmospheric Research, Boulder, Colorado

(Manuscript received 4 June 2007, in final form 13 December 2007)

ABSTRACT

The influence of the Indonesian Throughflow (ITF) on the dynamics and the thermodynamics in the southwestern Indian Ocean (SWIO) is studied by analyzing a forced ocean model simulation for the Indo-Pacific region. The warm ITF waters reach the subsurface SWIO from August to early December, with a detectable influence on weakening the vertical stratification and reducing the stability of the water column. As a dynamical consequence, baroclinic instabilities and oceanic intraseasonal variabilities (OISVs) are enhanced. The temporal and spatial scales of the OISVs are determined by the ITF-modified stratification. Thermodynamically, the ITF waters influence the subtle balance between the stratification and the mixing in the SWIO. As a result, from October to early December an unusual warm entrainment occurs, and the SSTs warm faster than just net surface heat flux–driven warming. In late December and January, the signature of the ITF is seen as a relatively slower warming of SSTs. A conceptual model for the processes by which the ITF impacts the SWIO is proposed.

1. Introduction

Sea surface temperature (SST) variations in the southern Indian Ocean are generally modest, but they are significantly larger in the southwestern Indian Ocean (SWIO; Annamalai et al. 2003). In an analysis of observational data, Klein et al. (1999) reported that surface heat flux anomalies explain the basinwide warming over most of the tropical Indian Ocean, with the only exception being the SWIO. Masumoto and Meyers (1998) argued that the large SST variations in the SWIO are mainly attributable to the forced Rossby waves propagating in from the southeastern Indian Ocean (SEIO). Moreover, because of Ekman pumping the SWIO is an upwelling region, where the subsurface thermocline variability has a significant influence on SSTs (Murtugudde and Busalacchi 1999; Schott et al. 2002). Xie et al. (2002) further concluded that much of the SST variability in the SWIO is caused not by local winds or surface heat fluxes but rather by oceanic Rossby waves that arrive from the east and modify the temperature of the upwelled waters.

The oceanic intraseasonal variabilities (OISVs) have been shown by several recent studies to be important for the heat budget in the oceanic mixed layer because of their impact on horizontal heat transport and related nonlinear advective effects (Waliser et al. 2003, 2004; Jochum and Murtugudde 2005). In the southern Indian Ocean, Du et al. (2005) studied the seasonal mixed layer heat budget by analyzing a high-resolution OGCM and concluded that maximum upwelling occurred when the Indonesian Throughflow (ITF) reached its annual maximum. Moreover, the warm advection associated with the ITF in their model neutralized the cold upwelling, leading to a slight damping of SST variability off Java and Sumatra (also see Murtugudde et al. 1998). They also found that the residual heat flux in their OGCM was not negligible during boreal winter, which might be attributable to the local intraseasonal variations. By comparing the model runs with open and closed ITF, Hirst and Godfrey (1993) noted that maximum temperature and salinity perturbations occur along the thermocline in the open ITF

Corresponding author address: Lei Zhou, Computer and Space Sciences Bldg. 2330, University of Maryland, College Park, College Park, MD 20742.
E-mail: lzhou@atmos.umd.edu

DOI: 10.1175/2007JPO3851.1

run in the region between 28° and 8°S, in addition to a strong vertical velocity shear.

To the best of our knowledge, there have been very few observational and modeling studies of OISVs thus far in the SWIO (e.g., Murtugudde and Busalacchi 1999). We showed in Zhou et al. (2008, hereafter ZMJ08) that the OISVs are strong from October to January, when they are mainly strengthened by baroclinic instabilities. Some interesting questions remain unexplored. Because the OISVs in the SWIO are hypothesized to originate in the east (Xie et al. 2002; ZMJ08), what is the relation between the ITF and the OISVs in the SWIO? Do the OISVs in the SWIO have a significant impact on local SST variability? In this study, we attempt to address these questions by analyzing an OGCM output along with the *World Ocean Atlas* (*WOA*) data (Conkright et al. 2002).

In section 2, the model is described and compared with satellite SST products (comparisons to altimeter data were presented in ZMJ08). In section 3, the westward propagation of ITF waters and its primary influence in the SWIO is examined, and in section 4 the dynamical influence of the ITF on the SWIO is discussed. Section 5 discusses the thermodynamic influence of the ITF, focusing on SST variability and the unusual warm entrainment. A conceptual model for the influence of ITF in the SWIO, along with further discussion and conclusions, is presented in section 6.

2. Model description and comparison

The SWIO has noticeably large OISVs (Waliser et al. 2003; Jochum and Murtugudde 2005), which are mainly attributable to oceanic internal baroclinic instabilities (ZMJ08). The wind forcings used here are weekly mean climatologies that retain very little energy in the intraseasonal band, consistent with the hypothesis that the OISVs are generated internally by the ocean. Interannual variability in the atmospheric intraseasonal variabilities (AISVs) may in fact modulate these OISVs, especially because the oceanic background state itself varies on interannual time scales. To simplify the analyses, it is assumed that the interannual variability in the AISV forcing will not significantly affect the basic processes of oceanic internal instabilities or the generation of OISVs. SST anomalies associated with the OISVs are a significant fraction of the total SST variability in the SWIO, which supports our assumption (Jochum and Murtugudde 2005). Therefore, this paper focuses on climatological model outputs from which the responses to the intraseasonal atmospheric forcing are largely removed.

The model used is a reduced-gravity, sigma-coordinate, primitive equation OGCM, with a horizontal resolution of 1/3° latitude and 1/2° longitude over the Indo-Pacific domain covering 30°S–30°N, 32°E–76°W (Murtugudde et al. 1996, 1998). There are 15 sigma layers in the vertical below the variable-depth mixed layer with a resolution of ~15 m in the thermocline in the SWIO, so vertical oscillations in the interior ocean can be adequately resolved. The surface mixed layer is determined by the hybrid mixing scheme of Chen et al. (1994), which explicitly accounts for the entrainment induced by the surface turbulent kinetic energy, shear-driven dynamic instability mixing, and convective mixing to remove static instabilities. The last sigma-layer thickness is a prognostic variable, whereas the other sigma layers are specified constant fractions of the total depth below the mixed layer to the motionless abyssal layer. The temperature and salinity from the climatological *WOA* data (Conkright et al. 2002) are interpolated onto the sigma layers, and the model temperature and salinity are relaxed to the interpolated WOA data in the sponge layer (south of 25°S) with a time scale of 5 days. The model is driven by the climatological weekly National Centers for Environmental Prediction (NCEP) Reanalysis winds as mentioned above (see Murtugudde et al. 2000 for details), with the surface heat fluxes computed by an advective atmospheric mixed layer model that allows SSTs to be directly determined by the variables internally calculated in the model, such as the air temperature and humidity (Seager et al. 1995; Murtugudde et al. 1996). The model outputs for all the analyses presented here are weekly mean fields from the last 20 yr of a 270-yr simulation.

The OGCM has been reported in many previous applications, demonstrating its ability to simulate the ocean dynamics and thermodynamics reasonably well in the tropical oceans. Mean SSTs (temperatures of the surface mixed layer in the model) and standard deviations (STDs) of the model outputs and the gridded Advanced Very High Resolution Radar (AVHRR) data (McClain et al. 1985) are shown in Fig. 1. Model simulations match satellite observations very well in the tropics; e.g., the 28°C isotherm in the model, which is the critical threshold for the occurrence of deep convection in the atmosphere, is almost identical to observations. However, there are obvious cold biases, as in the Bay of Bengal, where simulated SSTs are generally cooler than the observations by ~0.5°C. Maximum cold bias (~1°C) occurs between 10° and 20°S, centered at 15°S, 70°E. STDs of the SSTs are generally small (<1°C) in the tropical Indian Ocean, where the SSTs are higher than 28°C. In the SWIO, STDs are generally larger than 1.5°C. Moreover, large STDs to the northwest of Australia and around the northern tip of Madagascar are also well resolved. These simulated features

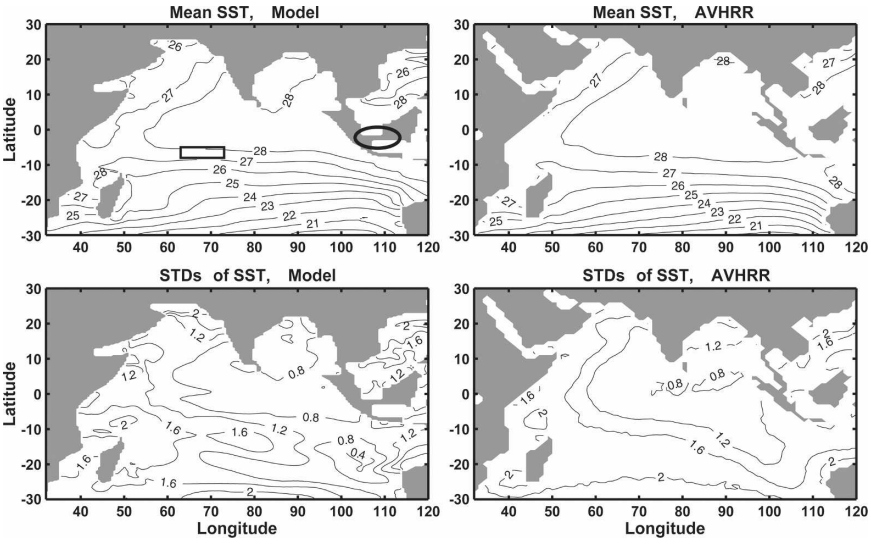

FIG. 1. Mean SSTs (°C) of (a) the 20-yr model outputs and (b) AVHRR data averaged from 1992–2005. (c),(d) Same as (a),(b), but for the STDs. The contour interval for the mean SSTs is 1°C and for the STDs is 0.4°C. The SWIO, which is defined as a rectangular region from 5° to 8°S and from 63° to 73°E, is identified by a thick rectangle in (a). The Karimata Strait, which is open in the Java run, is identified by an oval in (a).

are consistent with observations. However, SST variances are smaller than observations in the western Arabian Sea and the northern Bay of Bengal by ~0.5°C and also around 20°S, 80°E by ~1°C. Small SST variances are mainly attributable to the removal of AISVs from the external wind forcing.

The local maximum in SST variance centered around 12°S, which is attributable to the internal variability of the Indian Ocean, has been discussed in Jochum and Murtugudde (2005). In this paper, we focus on the variabilities in the SWIO, which is identified by a rectangle in Fig. 1a. The cold bias and small SST variance to the south of 10°S do not have a significant impact on the following discussions. We conclude that the model performance is acceptable for this study in the low latitudes in the Indian Ocean.

3. Westward propagation of the ITF waters

a. Indonesian Throughflow in the model

Although there is no precise or universally accepted definition of ITF, observational estimates have typically focused on zonal geostrophic transports between Java and Australia in the upper ocean (Meyers 1996). A similar measure was used to demonstrate the impact of ITF in the Indian Ocean dynamics and thermodynamics in Murtugudde et al. (1998). The zonal transport in the model, averaged down to 400 m between 10° and 15°S along 114°E, reaches a maximum of 15 Sv (1 Sv $\equiv$ 10^6 m^3 s^{-1}) in August with an annual mean of about 7 Sv, as in Murtugudde et al. (1998). This is slightly smaller than the commonly accepted value of 10 Sv (Gordon 2001) but is well within the uncertainty of the observational and model estimates (Godfrey 1996). The ITF waters at different depths follow different trajectories in the Indian Ocean (Song et al. 2004; Murtugudde et al. 1998). Only the upper-layer transports (above ~150 m) are confined to 20° and 8°S, with further significant influence on the mixed layer in the SWIO, as discussed below. Deeper ITF waters, especially below 500 m, mainly flow southward and circulate poleward to 15°S (Song et al. 2004). Therefore, in this study we only focus on simulated ITF in the upper 150 m, which we examine further below.

In the upper 150 m, we calculated the potential density; the Ertel potential vorticity (EPV), which is defined as $(f + \zeta)/\rho)(\partial\theta/\partial z)$, where f is the Coriolis parameter, ζ is the relative vorticity, ρ is the density, and θ is the potential temperature; and the zonal temperature advection $-u(\partial T/\partial x)$, where u is the zonal velocity and T is the temperature. The potential density σ_0, which is associated with the strong westward velocities from July to September (Fig. 2a), varies from 22.9 to 23.3 (Fig. 2b); the EPVs are smaller than 2×10^{-3} potential vorticity unit (PVU; 1 PVU $\equiv 10^{-6}$ K m^2 kg^{-1} s^{-1}; Fig. 2c); and the warm zonal advection occurs below the surface between 50 and 100 m (Fig. 2d). The water mass ranging in potential density from 22.9 to 23.3 can be tracked from the SEIO to the SWIO as shown in the temperature–salinity (T–S) diagram (de-

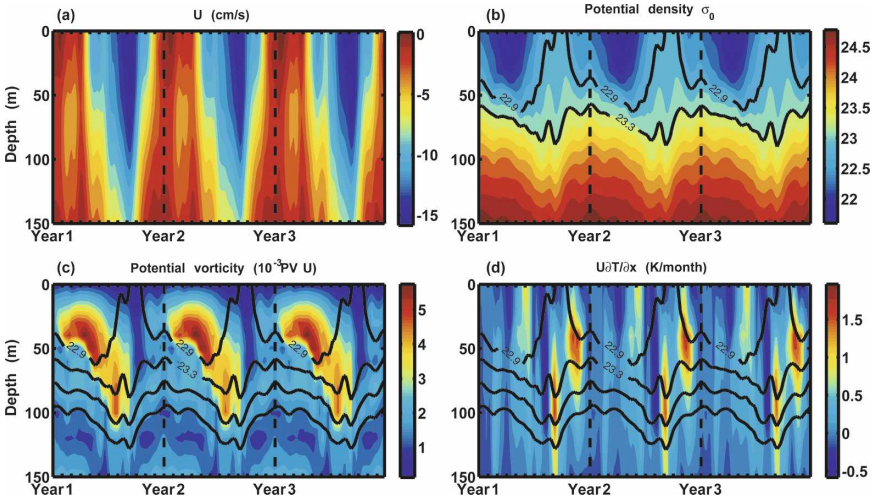

FIG. 2. (a) Zonal velocity, (b) potential density, (c) EPV, and (d) zonal temperature advection averaged from 10° to 15°S along 114°E over 3 yr.

picted as crosses in Fig. 3). To the east of 100°E, this water mass is not clearly separable from the ambient water (black and blue circles in Fig. 3) because of a strong mixing in the Indonesian seas (Meyers 1996; Murtugudde et al. 1998). To the west of 100°E, the ITF waters in the upper layer are distinguishable from the ambient Indian Ocean water. The density of the water mass continues to increase during its westward journey because of mixing with the denser ambient Indian Ocean water (Fig. 3). The pathway of the water mass is qualitatively consistent with the Lagrangian trajectory of the upper-layer ITF water shown in Song et al. (2004).

b. *Westward propagation of the ITF waters*

Because the subsurface ITF waters are far from the surface and the lateral boundaries, there is no generation or destruction of potential vorticity once they enter

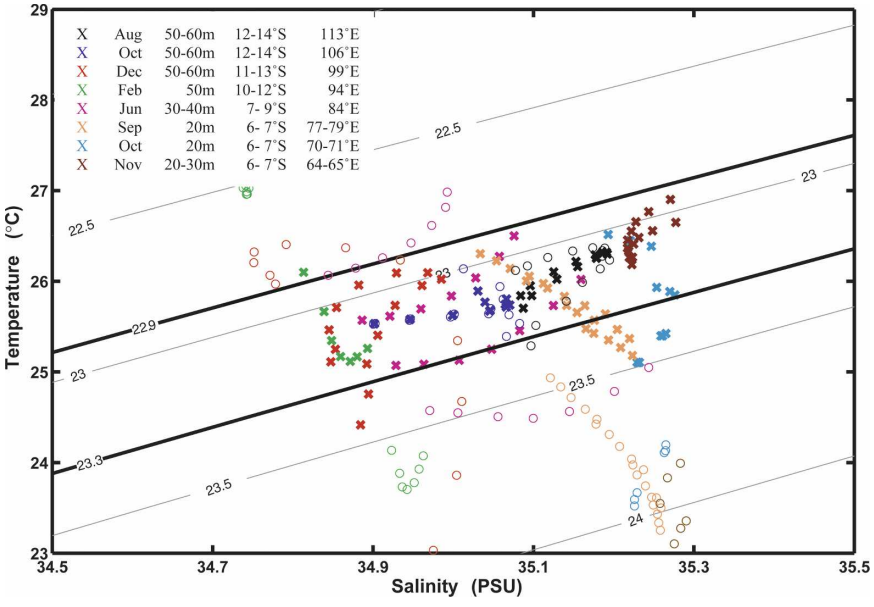

FIG. 3. A *T*–*S* diagram of the monthly 20-yr mean model outputs. The circles (crosses) represent the *T*–*S* at 20 m below (above). Each symbol represents *T*–*S* at one specific depth, lat, and lon, as shown in the legend. For example, the 12 black crosses represent the *T*–*S* properties at two layers (50 and 60 m), one lon point (113°E), and six lat points (from 12° to 14°S, with a lat resolution of 1/3°).

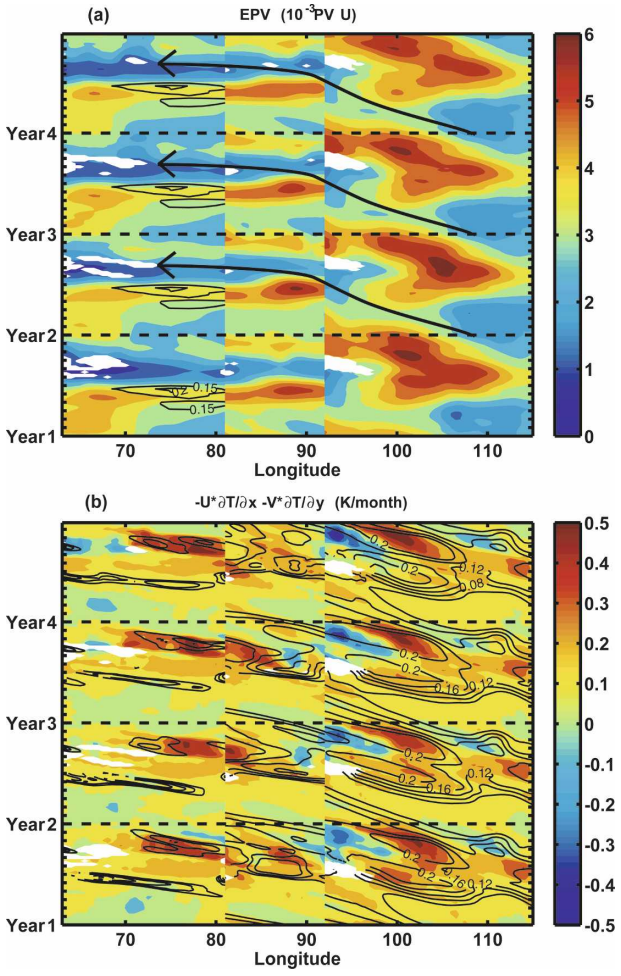

FIG. 4. (a) EPV and (b) horizontal temperature advection projected onto the surface of $\sigma_0 = 23.3$ along 6°S from 63° to 81°E, along 8°S from 81° to 92°E, and along 12°S from 92° to 115°E, smoothed with 5° zonal running mean. The lat shift from 12° to 6°S follows the spreading of ITF waters shown in Fig. 3. The contours in (a) are the wind stress curl (10^{-6} Pa m^{-1}) and the contours in (b) are the zonal velocities on the $\sigma_0 = 23.3$ surface in m s^{-1}.

the Indian Ocean. Therefore, by projecting the EPV and the horizontal temperature advection onto the $\sigma_0 = 23.3$ surface and following the pathway shown in Fig. 3, one can also track the small EPV ($<2 \times 10^{-3}$ PVU) and warm advection associated with the ITF from the east to the west across the Indian Ocean Basin. Because the ITF water does not propagate strictly westward, especially between 80° and 100°E (Fig. 3), in the interest of accuracy the horizontal temperature advection $-u(\partial T/\partial x) - v(\partial T/\partial y)$ (where v is the meridional velocity) is shown in Fig. 4b, even though the zonal temperature advection $-u(\partial T/\partial x)$ generally dominates. The warm ITF waters are carried westward by the south equatorial currents, as shown with the contours in Fig. 4b. The westward spreading rate of the ITF waters is about 20 cm s^{-1} in the SEIO, but slightly slower in the SWIO (~15 cm s^{-1}). The values of σ_0 at the sea surface are larger than 23.3 in the blank regions between 63° and 73°E in Fig. 4, implying that very strong diapycnal mixing can blur the distinction between the ITF water and the ambient Indian Ocean water (see section 4). These regions are also where the warm horizontal advection carrying the ITF waters ends, which suggests that the warm subsurface waters are entrained into the surface mixed layer (see section 5a for a detailed discussion). The westward spreading of the ITF waters in the model is given in Fig. 4 and is discussed below.

c. *The primary influence of the ITF waters on the SWIO*

There is a thermocline ridge in the SWIO that is maintained by the Ekman pumping. When the ITF waters reach this region, they significantly affect the vertical structure. Because the ITF waters are warmer and more buoyant than the ambient waters, they reduce the vertical stratification and the stability in the upper layer from August to December (Fig. 5a). The modification of the vertical structure is mainly attributable to the temperature effect of the ITF waters because the Brunt–Väisälä frequency (N) and the vertical temperature gradients are close to each other (Fig. 5a). Although the ITF waters are also fresher than the ambient waters, the salinity difference is so small that its effect on the vertical stratification is negligible (also see Hirst and Godfrey 1993). The vertical temperature gradients and N in the upper layer reach their minimums simultaneously in October and early November. Meanwhile, they become larger between the subsurface and the cold deep ocean waters because of warm advection. The vertical variation of N and the temperature gradients from August to early December can also be detected in the monthly high-resolution (1/4°) WOA data (Conkright et al. 2002; Boyer et al. 2005), shown in Fig. 5b. In summary, the primary influence of the ITF waters on the SWIO is to reduce the vertical stratification, which in turn leads to significant impacts on the dynamics and thermodynamics in the SWIO, as discussed in the following two sections.

To highlight the primary influence of the ITF on the SWIO, we made another test (referred to as the Java run) with the Karimata Strait open (the strait connecting the South China Sea and the Java Sea, identified with an oval in Fig. 1a) and rest of the model configuration unchanged. The model run which we focused on in this paper is referred to as the control run. As predicted in Gordon et al. (2003), in boreal winter the

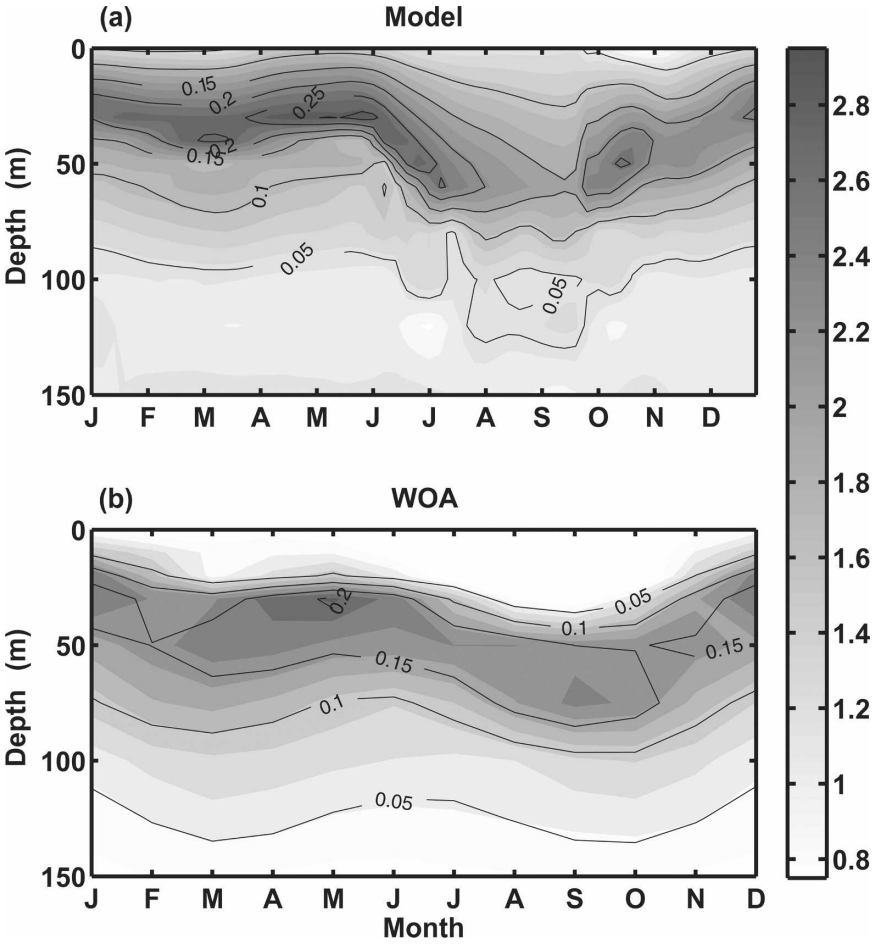

FIG. 5. (a) Mean N (shades in 10^{-2} s^{-1}) and the vertical temperature gradient (K m^{-1}) within a rectangular region 6°–7°S, 63°–73°E, calculated with the model outputs. (b) The same as (a), but calculated with the monthly high-resolution *WOA* data.

intrusion of fresh surface waters from the Java Sea into the southern Makassar Strait leads to cool SSTs in the Indian Ocean; meanwhile, thermocline intensification of the ITF is enhanced (Tozuka et al. 2007). This seasonal variability is well resolved in the Java run. Thus, the contrast between the subsurface warm ITF water and upper Indian Ocean water is more distinct in the Java run, as can be seen in the vertical profile of N (not shown). From July to December, the Brunt–Väisälä frequency in the Java run is smaller (larger) than it is in the control run above (below) the thermocline. Therefore, the stability of the upper layer in boreal winter is reduced more in the Java run than it is in the control run. As a result, the intraseasonal variabilities of SSTs and sea surface heights (SSHs) in the SWIO are stronger in the Java run than they are in the control run (Fig. 6) in boreal winter. These comparisons support the hypothesis that ITF exerts direct influence on the SWIO as discussed above.

4. Influence of ITF on the dynamics in the SWIO: Scale selection

In the SWIO, the reduced vertical stratification by the ITF waters favors the baroclinic instability. As a result, the baroclinic energy conversions and the OISVs are enhanced in boreal winter, as shown in ZMJ08. Because the subsurface ITF waters are away from the boundaries, their potential vorticity is conserved during the westward propagation. Following the Eady model described in Vallis (2006; see our appendix for details), the maximum growth rate of the baroclinically unstable wave is $\sigma_{\max} \approx 0.3U/L_d$, where U is the basic flow and L_d is the Rossby radius of deformation; and the corresponding wavelength of the most unstable wave is $L_{\max} \approx 3.9L_d$. The $L_{\max}$ and $\sigma_{\max}$ are calculated with the model outputs and shown in Fig. 7. In the SWIO, the wavelength of the maximum instability is 500–600 km, which is very close to the wavelength of the OISVs

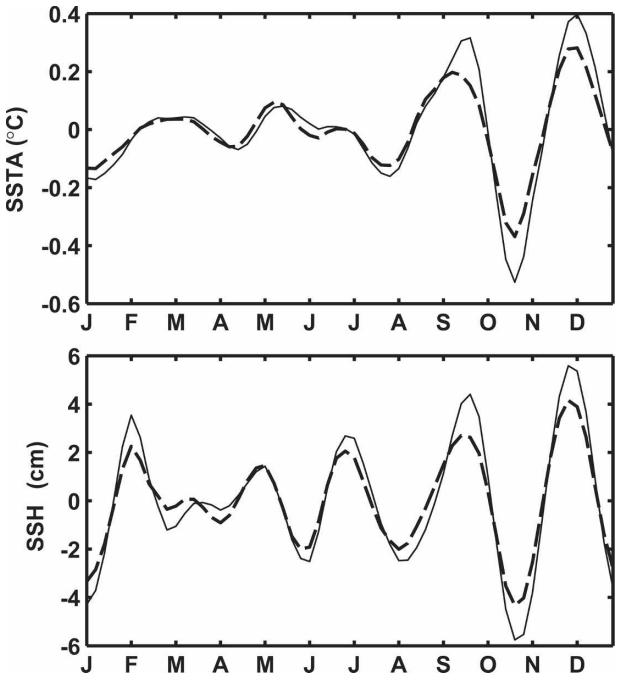

FIG. 6. The intraseasonal SSTAs and SSHs averaged in the SWIO (6°–7°S, 63°–73°E) in the Java run (solid line) and the control run (dashed line).

in the SWIO (~650 km; ZMJ08). The period corresponding to the maximum growth rate is mainly 40–100 days, which is the typical intraseasonal band. Although the theoretical estimates are relatively simple and idealized, they reveal that the dynamical influence of the ITF waters in the SWIO is primarily to reinforce the baroclinic instability and the OISVs by reducing the stratification. Furthermore, the ITF-modified stratification determines the Rossby radius of deformation L_d (the Coriolis parameter and the water depth can be considered as invariable) and thereby determines the time and length scales of the OISVs in the SWIO.

5. Influence of ITF on the SSTs in SWIO

SST variability in the SWIO is dominated by the net surface heat flux Q_{net}, as shown in Fig. 8. From April to September, the correlation between them is as high as 0.97. However, there are also obvious seasonally dependent discrepancies between Q_{net} and the SST variability. From October to early December, SSTs warm faster than Q_{net}, and in late December and January, they warm more slowly. The former difference can clearly be attributed to zonal advection and entrainment, which are significantly influenced by the ITF as discussed in section 5a, but the latter difference is assumed to have only an indirect connection with the ITF (discussed in section 5b).

a. Fast warming SSTs from October to early December

Hirst and Godfrey (1993, 1994) concluded that only in regions with strong upwelling and convective mixing can SSTs be dramatically affected by subsurface temperature perturbations generated by the ITF. The

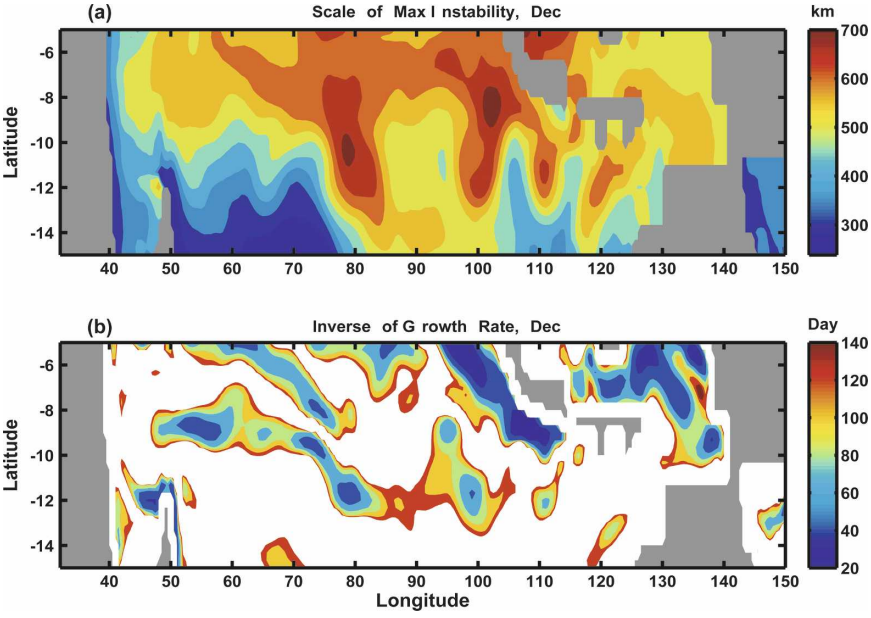

FIG. 7. (a) Wavelength of the maximum instability ($L_{\max} = 3.9L_d$) and (b) the inverse of the corresponding maximum growth rate ($\sigma_{\max} = 0.3U/L_d$), both in December.

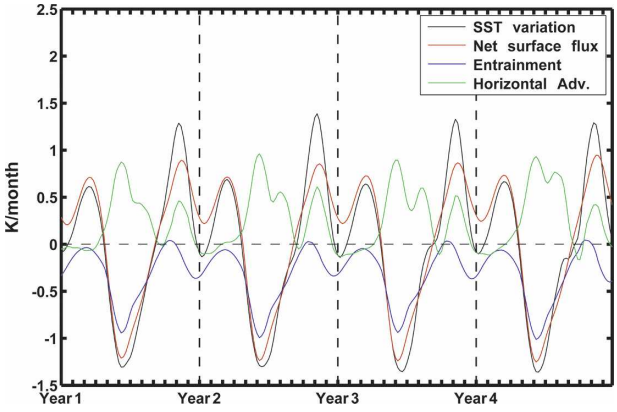

FIG. 8. SST variation, net surface heat flux, entrainment, and horizontal temperature advection averaged within a rectangular region 6°–7°S, 63°–73°E and smoothed with the 1-month running mean. Positive (negative) values mean that the upper mixed layer gains (loses) heat.

SWIO is just such a region. Because of Ekman pumping, it is an open-ocean upwelling region that is characterized by a shallow thermocline (Reverdin 1987; Murtugudde and Busalacchi 1999; Schott et al. 2002). Meanwhile, surface turbulent kinetic energy tends to deepen the mixed layer, leading to significant entrainment as a contribution to the mixed layer heat budget. The correlation between entrainment and SST variability is 0.8 (Fig. 8). In October, after the warm ITF waters reach the SWIO, the water column from 30 to 70 m (centered at ~55 m), which is just beneath the mixed-layer bottom, is significantly warmed (Fig. 9). Thus, rather nonintuitively, entrainment acts to warm the mixed layer rather than cool it (Fig. 8).

The anomalous warm entrainment is usually associated with a barrier layer structure, which is an isothermal layer below the density-stratified surface mixed layer (Lukas and Lindstrom 1991; Sprintall and Tomczak 1992), and serves to decouple the mixed layer thermodynamics and dynamics. There are multiple processes responsible for the barrier layer formation. For example, Schiller and Godfrey (2003) found that in the central and eastern tropical Indian Ocean, the barrier layer occurs because of the long-term freshwater gains at the surface. Meanwhile, penetrative solar radiation heats the water below the shallow mixed layer during the clear and calm phase of an intraseasonal event. As a result, a vertical temperature inversion occurs, leading to the warm entrainment. We calculated the barrier layer according to the definition of Sprintall and Tomczak (1992) with the weekly model outputs. The large penetrative solar heating and the barrier layer formation are captured in the central and eastern tropical Indian Ocean (Fig. 10). However, in the SWIO, penetrative heating rates are smaller than 0.1 K month^{-1} in October. The mixed layer is quite deep, and there is almost no barrier layer (also see Murtugudde and Busalacchi 1999) because the salinity effects on the stratification are negligible (Hirst and Godfrey 1993). Therefore, the genesis mechanism of warm entrainment in the SWIO is distinct from what was discussed in Schiller and Godfrey (2003). Rather than being heated by the solar penetration, the waters beneath the mixed layer in the SWIO are warmed by the warm ITF waters originating from the SEIO from October to early December (Fig. 9). Moreover, there are cyclonic eddies in the SWIO (ranging from 70° to 60°E around 8°S), which lead to increased entrainment and SST disturbance (Fig. 11). Consequently, the subsurface warm waters are entrained into the surface mixed layer, leading to fast warming of SSTs. Subsurface warming and the

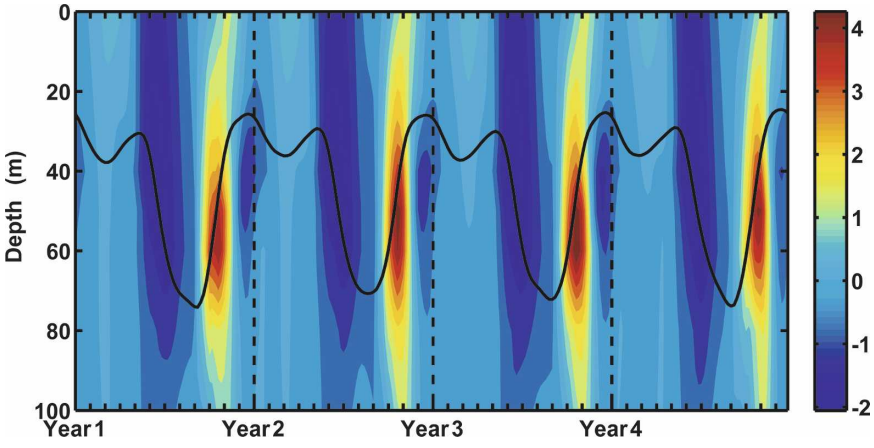

FIG. 9. Temperature variations (see color codes, K month^{-1}) and mixed layer depth (solid line), averaged in the region of 6°–7°S, 63°–73°E.

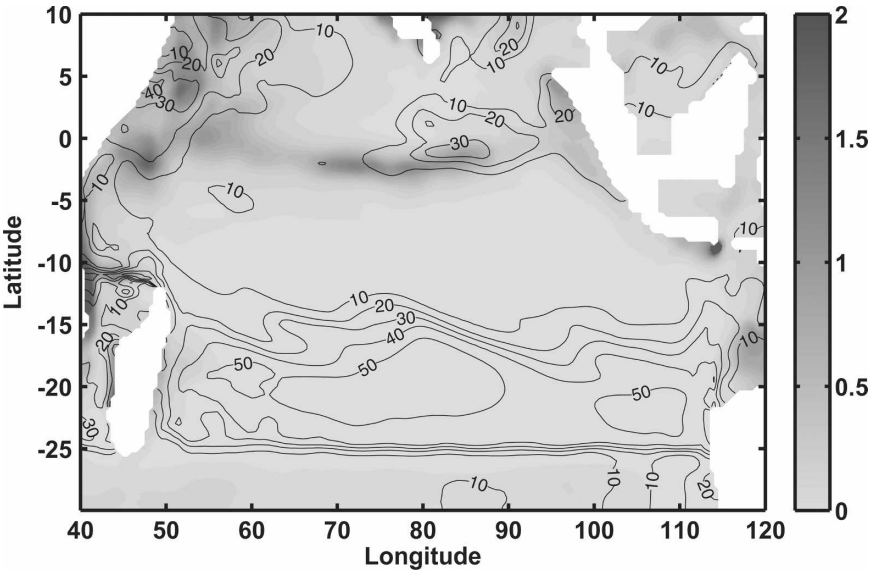

FIG. 10. Solar radiation penetration heating rates (shading, K month^{-1}) and the barrier layer depth (contours, m) in October.

weakening of the stratification tend to enhance the mixed layer deepening and entrainment. During this process, strong diapycnal mixing blends the ITF waters and the ambient Indian Ocean waters to the extent that the ITF waters lose their *T*–*S* properties (blank regions in Fig. 4). Therefore, the influence of the ITF on SSTs in the SWIO depends on a subtle balance between the stratification and mixing.

Please note that because the subsurface ITF waters are warmer than the Indian Ocean waters above, temperature inversions do exist in the model outputs. However, the inversions are too weak to initiate the vertical convection by themselves. Eddy kinetic energy (EKE, provided by the baroclinic instability) is still required to break the isopycnal surface and entrain the ITF waters into the upper mixed layer.

b. *Slow warming SSTs in late December and January*

The fast warming of SSTs from October to early December is thus attributable to the westward propagation of the warm ITF waters and the subsequent warm entrainment, as discussed above. The warming of SSTs, however, is slower than expected from Q_{net} from late December to January, as seen in Fig. 8. This difference is attributed to the indirect influence of the injection of ITF waters on local vertical processes.

The ITF waters lose their warmer and fresher character during the strong diapycnal mixing from October to early December. Therefore, from late December into January, the subsurface waters significantly cool, and the normal vertical stratification resumes (Fig. 9). However, the OISVs enhanced by the ITF-related baroclinic instability still persist during this time, albeit in their decaying phase (ZMJ08). Therefore, the remaining OISVs provide sufficient EKE to sustain the cold entrainment, which cools the SSTs or, alternatively, slows the rate of warming. After January, the OISVs dissipate completely and no EKE is available to drive entrainment, which results in near-zero entrainment in February and March. Therefore, the slow warming of SSTs in the SWIO in late December and

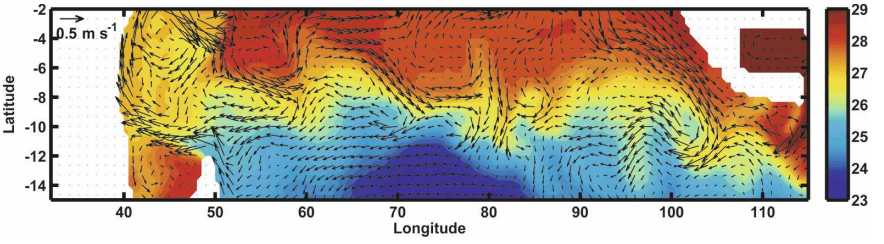

FIG. 11. Weekly mean SSTs (see color codes, °C) and surface velocities (vectors) during 16–21 Nov of year 7, when the warm entrainment reaches its maximum.

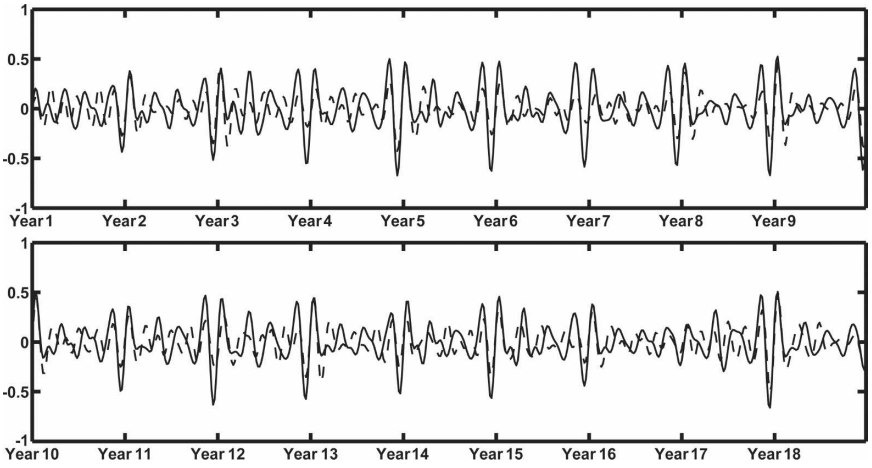

FIG. 12. Intraseasonal entrainment (solid line, K month^{-1}) and intraseasonal SSHAs (dashed line 10 cm) at 8°S, 63°E for 18 yr.

January is attributable to the vertical processes influenced by the intrusion of remote ITF waters into the region.

Pronounced cold entrainment from April to June is likely to be attributable to local Ekman pumping associated with the pronounced wind stress curl (contours in Fig. 4a). However, its influence on the upper-layer heat budget is largely neutralized by the meridional warm temperature advection associated with the southward Ekman transport (note the large westward velocities at this time in Fig. 4b). Thus, advection has no significant net impact on the SSTs, and the SST variation is mainly controlled by Q_{net} (Fig. 8). The local processes at this time of the year are not directly related to the ITF, so the details of this cold entrainment are not discussed further here.

c. *Relations between thermodynamics and dynamics in the intraseasonal band*

ITF waters can influence both the dynamics and thermodynamics in the SWIO by modifying the vertical stratification as discussed above. Because the maximum growth rate of the unstable waves is in the intraseasonal band and the entrainment is partly sustained by the EKE generated by the baroclinic instability, intraseasonal entrainment and intraseasonal sea surface height anomalies (SSHAs) have high correlations, especially in boreal winter of each year. For example, at 8°S, 63°E, their correlation is 0.6 (Fig. 12). Actually, the correlation between the two is large both in the SWIO and the SEIO, where the OISVs and the entrainment are closely related to the ITF (Fig. 13; Du et al. 2005; Yu and Potemra 2006; ZMJ08). Therefore, in the SWIO there is a close relation between the thermodynamics and the dynamics in the intraseasonal band, which is responsible for the relatively persistent Bjerknes feedback in this region (Annamalai et al. 2003, 2005). It should be possible to estimate the intraseasonal heat fluxes associated with these processes, which are not easily observed. But observed quantities such as the intraseasonal SSHAs can be used in inverse calculations to elucidate the coupled climate interactions in the region, which are of significant importance for the rim countries (e.g., Xie et al. 2002).

6. Discussion and conclusions

When the ITF waters reach the SWIO from August to early December, their primary effect is to reduce the vertical stratification, which favors baroclinic energy conversions. Consequently, the OISVs are enhanced (ZMJ08), and their temporal and spatial scales are determined by the ITF-modified stratification. The ITF also has a significant influence on the SSTs in the SWIO. From October to early December, the warm ITF waters heat the subsurface waters, leading to an unusual warm entrainment that speeds up the SST warming. From late December to January, the warm ITF waters disappear because of the strong diapycnal mixing driven by the baroclinic instability, and the subsurface waters become cool. However, the OISV activity still exists and supplies the EKE to drive cold entrainment, leading to a relatively slow warming of the SSTs. These processes are attributable to the ITF impact on local processes.

In reality, we believe that the above influence of the ITF waters in the SWIO can be even more pronounced if mixing rates are smaller (most models incur excess mixing) and if eddies are resolved explicitly. Gordon et al. (2003) found that during boreal winter, cold water

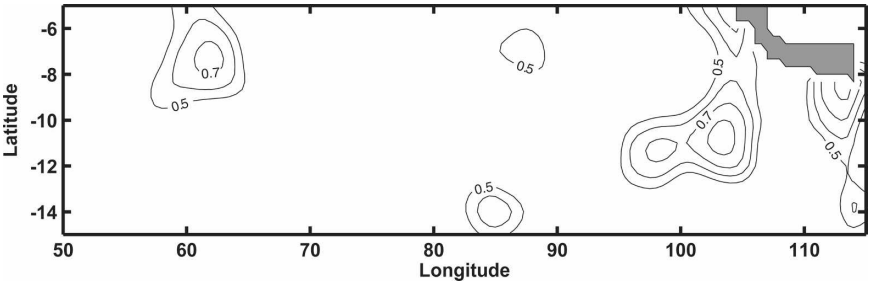

FIG. 13. Correlations between the intraseasonal entrainment and the intraseasonal SSHAs, which are statistically significant at the 95% confidence level.

flows from the Java Sea into the southern Makassar Strait, preventing the warm Pacific water from entering the Indian Ocean and leading to cooler SSTs in the Indian Ocean. Therefore, the warm subsurface waters are more distinguishable from the ambient Indian Ocean water when they reach the SWIO. Moreover, the wind energy is mainly captured by the second baroclinic mode currents in the SEIO (Iskandar et al. 2006), which can supply more energy to the subsurface westward propagation of the ITF waters.

In summary, we propose that in reality the southern Makassar Strait is like a valve through which the cold waters from Java Sea flow into the southern Makassar Strait, making the subsurface warm advection of ITF more distinct compared to the relatively cool Indian Ocean SSTs. The winds over the SEIO are like a propeller that supplies energy to the subsurface warm advection in the ocean. The ITF is like a conveyor belt that carries the variabilities from the SEIO to the SWIO, and the SWIO is like a mixer during boreal winter, when the subsurface water is mixed up into the upper mixed layer and the SSTs are modulated. These processes are sketched in Fig. 14. Of course, these processes require more validation against observations and model simulations.

As shown in Song and Gordon (2004), the vertical structure of ITF has a significant impact on the stratification and surface heat flux in the Indian Ocean. Potemra et al. (2002) found that the vertical structure of the ITF has a large temporal variability. This study argues that the spreading and mixing of the ITF water and its influence on the southern Indian Ocean have a significant seasonal variability. An interesting question still unresolved now is whether the ITF leads to enhanced or diminished ocean heat gain (Song et al. 2004) from the atmosphere. Godfrey (1996) suggested less ocean heat gain, assuming that the temperature of the upwelling water is increased when the ITF is open, and Vranes et al. (2002) suggested increased heat gain, arguing that the transport-weighted temperature of the ITF tends to be cooler than the ambient Indian Ocean thermocline water. We do not intend to settle this issue by analyzing the present model outputs alone. Nonetheless, based on the model results, it is very likely that the influence of the ITF on the ocean heat gain depends on the seasonal variability of the subtle balance be-

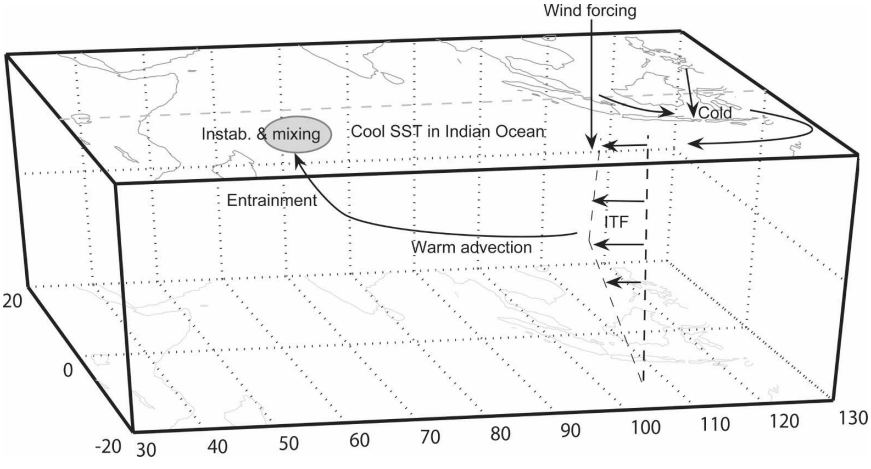

FIG. 14. Sketch of the influence of ITF on the SWIO.

tween the stratification and the mixing. The SSTs warm relatively faster from October to December, which suggests a reduced heat gain, and the SST warming is slower in late December into January, which should drive an enhanced heat gain. The role of these processes in the coupled climate variability remains to be explored.

Acknowledgments. This work was supported by NASA Indian Ocean Mesoscale Funding and NOAA Coupled Mesoscale Funding. We deeply appreciate the assistance of James Beauchamp and Eric Hackert in the preparation of model outputs. We also thank two anonymous reviewers for their comments and suggestions. Zhou gratefully acknowledges his NASA Earth System Science Fellowship.

APPENDIX

The Eady Model

Because the subsurface ITF waters are away from the sea surface and the lateral boundaries, their potential vorticities are conserved after they enter the Indian Ocean until they are entrained into the upper mixed layer in the SWIO (Fig. 4a). Following Vallis (2006), the conservation equation of the potential vorticity is

$$\left(\frac{\partial}{\partial t} + U\frac{\partial}{\partial x}\right)\left(\nabla^2\Psi + \frac{H^2}{L_d^2}\frac{\partial^2\Psi}{\partial z^2}\right) = 0,$$

where U is the basic flow, Ψ is the streamfunction, H is the water depth, $L_d = NH/f$ is the Rossby radius of deformation, N is the Brunt–Väisälä frequency, and f is the Coriolis parameter. The boundary conditions are

$$\left(\frac{\partial U}{\partial z}z - c\right)\frac{\partial\Psi}{\partial z} - \frac{\partial U}{\partial z}\Psi = 0, \quad z = 0, H,$$

$$\Psi = 0, \quad \text{and} \quad y = 0, L.$$

Assuming the wavelike solution in both x and y directions, that is,

$$\Psi(x, y, z, t) = \psi(z)\sin ly e^{ik(x-ct)},$$

we obtain the dispersion relation of the Eady waves

$$c = \frac{U}{2} \pm \frac{U}{\mu}\left[\left(\coth\frac{\mu}{2} - \frac{\mu}{2}\right)\left(\frac{\mu}{2} - \tanh\frac{\mu}{2}\right)\right]^{1/2},$$

where $\mu = kL_d$. The instability occurs when $\mu > 2.4$. The corresponding growth rate is

$$\sigma = c_i k = \frac{U}{L_d}\left[\left(\coth\frac{\mu}{2} - \frac{\mu}{2}\right)\left(\frac{\mu}{2} - \tanh\frac{\mu}{2}\right)\right]^{1/2},$$

where c_i is the imaginary part of c. The meridional wavenumber is omitted in the growth rate because it is much smaller than k. The maximum growth rate occurs when $\mu_{\max} = 1.61$. Accordingly, the wavelength of the maximum instability is $L_{\max} = (2\pi/k) = (2\pi L_d/\mu_{\max}) \approx 3.9L_d$, and the corresponding maximum growth rate is $\sigma_{\max} \approx 0.3U/L_d$.

REFERENCES

Annamalai, H., R. Murtugudde, J. Potemra, S. P. Xie, P. Liu, and B. Wang, 2003: Coupled dynamics over the Indian Ocean: Spring initiation of the zonal mode. *Deep-Sea Res. II,* **50,** 2305–2330.

——, J. Potemra, R. Murtugudde, and J. P. McCreary, 2005: Effect of preconditioning on the extreme climate events in the tropical Indian Ocean. *J. Climate,* **18,** 3450–3469.

Boyer, T., S. Levitus, H. Garcia, R. A. Locarnini, C. Stephens, and J. Antonov, 2005: Objective analyses of annual, seasonal, and monthly temperature and salinity for the World Ocean on a 0.25° grid. *Int. J. Climatol.,* **25,** 931–945.

Chen, D., L. M. Rothstein, and A. J. Busalacchi, 1994: A hybrid vertical mixing scheme and its application to tropical ocean models. *J. Phys. Oceanogr.,* **24,** 2156–2179.

Conkright, M. E., and Coauthors, 2002: *Introduction.* Vol. 1, *World Ocean Database 2001,* NOAA Atlas NESDIS 42, 160 pp.

Du, Y., T. Qu, G. Meyers, Y. Masumoto, and H. Sasaki, 2005: Seasonal heat budget in the mixed layer of the southeastern tropical Indian Ocean in a high-resolution ocean general circulation model. *J. Geophys. Res.,* **110,** C04012, doi:10.1029/2004JC002845.

Godfrey, J. S., 1996: The effect of the Indonesian Throughflow on ocean circulation and heat exchange with the atmosphere: A review. *J. Geophys. Res.,* **101,** 12 217–12 238.

Gordon, A. L., 2001: Interocean exchange. *Ocean Circulation and Climate,* G. Siedler et al., Eds., Academic Press, 303–314.

——, R. D. Susanto, and K. Vranes, 2003: Cool Indonesian Throughflow as a consequence of restricted surface layer flow. *Nature,* **425,** 824–828.

Hirst, A. C., and J. S. Godfrey, 1993: The role of Indonesian Throughflow in a global ocean GCM. *J. Phys. Oceanogr.,* **23,** 1057–1086.

——, and ——, 1994: The response to a sudden change in Indonesian Throughflow in a global ocean GCM. *J. Phys. Oceanogr.,* **24,** 1895–1910.

Iskandar, I., T. Tozuka, H. Sasaki, Y. Masumoto, and T. Yamagata, 2006: Intraseasonal variations of surface and subsurface currents off Java as simulated in a high-resolution ocean general circulation model. *J. Geophys. Res.,* **111,** C12015, doi:10.1029/2006JC003486.

Jochum, M., and R. Murtugudde, 2005: Internal variability of Indian Ocean SST. *J. Climate,* **18,** 3726–3738.

Klein, S. A., B. J. Soden, and N.-C. Lau, 1999: Remote sea surface temperature variations during ENSO: Evidence for a tropical atmospheric bridge. *J. Climate,* **12,** 917–932.

Lukas, R., and E. Lindstrom, 1991: The mixed layer of the western equatorial Pacific Ocean. *J. Geophys. Res.,* **96,** 3343–3357.

Masumoto, Y., and G. Meyers, 1998: Forced Rossby waves in the southern tropical Indian Ocean. *J. Geophys. Res.,* **103,** 27 589–27 602.

McClain, E. P., W. G. Pichel, and C. C. Walton, 1985: Compara-

tive performance of AVHRR-based multichannel sea surface temperatures. *J. Geophys. Res.,* **90,** 11 587–11 601.

Meyers, G., 1996: Variation of Indonesian Throughflow and the El Niño–Southern Oscillation. *J. Geophys. Res.,* **101,** 12 255–12 263.

Murtugudde, R., and A. J. Busalacchi, 1999: Interannual variability of the dynamics and thermodynamics of the tropical Indian Ocean. *J. Climate,* **12,** 2300–2326.

——, R. Seager, and A. Busalacchi, 1996: Simulation of the tropical oceans with an ocean GCM coupled to an atmospheric mixed-layer model. *J. Climate,* **9,** 1795–1815.

——, A. J. Busalacchi, and J. Beauchamp, 1998: Seasonal-to-interannual effects of the Indonesian Throughflow on the tropical Indo-Pacific basin. *J. Geophys. Res.,* **103,** 21 425–21 441.

——, J. P. McCreary Jr., and A. J. Busalacchi, 2000: Oceanic processes associated with anomalous events in the Indian Ocean with relevance to 1997–1998. *J. Geophys. Res.,* **105,** 3295–3306.

Potemra, J. T., S. L. Hautala, J. Sprintall, and W. Pandoe, 2002: Interaction between the Indonesian Seas and the Indian Ocean in observations and numerical models. *J. Phys. Oceanogr.,* **32,** 1838–1854.

Reverdin, G., 1987: The upper equatorial Indian Ocean: The climatological seasonal cycle. *J. Phys. Oceanogr.,* **17,** 903–927.

Schiller, A., and J. S. Godfrey, 2003: Indian Ocean intraseasonal variability in an ocean general circulation model. *J. Climate,* **16,** 21–39.

Schott, F., M. Dengler, and R. Schoenefeldt, 2002: The shallow overturning circulation of the Indian Ocean. *Prog. Oceanogr.,* **53,** 57–103.

Seager, R., M. B. Blumenthal, and Y. Kushnir, 1995: An advective atmospheric mixed-layer model for ocean modeling purposes: Global simulation of surface heat fluxes. *J. Climate,* **8,** 1951–1964.

Song, Q., and A. Gordon, 2004: Significance of the vertical profile of the Indonesian Throughflow transport to the Indian Ocean. *Geophys. Res. Lett.,* **31,** L16307, doi:10.1029/2004GL020360.

——, ——, and M. Visbeck, 2004: Spreading of the Indonesian Throughflow in the Indian Ocean. *J. Phys. Oceanogr.,* **34,** 772–792.

Sprintall, J., and M. Tomczak, 1992: Evidence of the barrier layer in the surface layer of the tropics. *J. Geophys. Res.,* **97,** 7305–7316.

Tozuka, T., T. Qu, and T. Yamagata, 2007: Dramatic impact of the South China Sea on the Indonesian Throughflow. *Geophys. Res. Lett.,* **34,** L12612, doi:10.1029/2007GL030420.

Vallis, G. K., 2006. *Atmospheric and Oceanic Fluid Dynamics: Fundamentals and Large-Scale Circulation.* Cambridge University Press, 745 pp.

Vranes, K., A. L. Gordon, and A. Ffield, 2002: The heat transport of the Indonesian Throughflow and implications for the Indian Ocean heat budget. *Deep-Sea Res.,* **49,** 1391–1410.

Waliser, D. E., R. Murtugudde, and L. Lucas, 2003: Indo-Pacific Ocean response to atmospheric intraseasonal variability. 1: Austral summer and the Madden–Julian Oscillation. *J. Geophys. Res.,* **108,** 3160, doi:10.1029/2002JC001620.

——, ——, and ——, 2004: Indo-Pacific Ocean response to atmospheric intraseasonal variability. 2: Boreal summer and the intraseasonal oscillation. *J. Geophys. Res.,* **109,** C03030, doi:10.1029/2003JC002002.

Xie, S.-P., H. Annamalai, F. A. Schott, and J. P. McCreary Jr., 2002: Structure and mechanisms of South Indian Ocean climate variability. *J. Climate,* **15,** 864–878.

Yu, Z., and J. Potemra, 2006: Generation mechanism for the intraseasonal variability in the Indo-Australian basin. *J. Geophys. Res.,* **111,** C01013, doi:10.1029/2005JC003023.

Zhou, L., R. Murtugudde, and M. Jochum, 2008: Dynamics of the intraseasonal oscillations in the Indian Ocean South Equatorial Current. *J. Phys. Oceanogr.,* **38,** 121–132.